

Chapter 1

Introduction

The phenomena associated with the radiation interaction in matter are commonly understood to include a wide variety of physical effects. Moreover, the nature of interactions in matter depends on the incoming type of radiation and energy.

Historically, the first nuclear particle detectors (like those based on X -rays films) were very simple. In the course of time, the detectors have evolved more and more. In addition, complex systems of detectors leading to large experimental apparatus often consist of several sub-detectors and require sophisticated methods of reconstruction and analysis of data to decrease the experimental errors. Therefore, both detectors and detection methods are fields of development and investigation.

In each application field, the detector configuration has to be designed for the collision geometry, i.e., the experimental apparatus has to be capable to process the particles emerging from the interaction or production volume. For instance, for medical applications, the detection system needs to be adapted to the part of the patient's body under examination. In most cases, the large amount of data to analyze, their variety and often the large energy range to be covered can only be handled by the construction of detectors composed of many sub-detectors assigned to dedicated tasks. For example, in high energy physics experiments, collisions between two particles beams (*collider type of collision*) or by a beam hitting a fixed target (*fixed target type of collision*) produce a variety of particles, most of the time with very complicated configurations of events. Space-based experiments are another example of application where detector development is needed. These experiments aim at the study of astrophysics, gamma rays astronomy and cosmic rays, interactions of cosmic rays with the space matter or with the Earth atmosphere or the detection of Galactic and extra-

Galactic photons. The achievement of such vast research programs requires very reliable apparatus.

In this chapter, an overview of the types of interactions in matter and the physical meaning of interaction cross section are presented. These interactions and their properties will be extensively discussed in the two following chapters from the phenomenological point of view. These features constitute fundamental principles for designing detection systems. In addition, the basic equations and relations of relativistic kinematics will be introduced. Finally, an overview of detection methods and detecting media will be given.

In the following chapters, the scintillation processes and scintillating media (Chapter 4), the *electron-hole* carriers formation and detection in semiconductors (Chapter 5), and the signal generation in ionization chambers (Chapter 6) will be dealt with. The principles of particle energy determination for both electromagnetic and hadronic particles are discussed in Chapter 7. In Chapter 8, droplet detectors and their response to neutrons and α -particles are discussed. In Chapter 9, detector applications for Medical Physics are considered.

1.1 Radiation and Particle Interactions

Radiation is detected by its interaction in matter. Every detection system has the same structure: it starts with the interaction of the radiation with the detection medium; the result of the interaction is transformed into signals, which are readout and usually recorded. The interaction processes depend on both the type and energy of the incoming particles* (or photons). The energy ranges encountered also vary by orders of magnitude. For example, the electromagnetic spectrum[†] (photons) covers many decades of frequencies. The situation is similar for charged particles. Their energy ranges from fractions of eV to 10^{20} eV, in the case of ultra-high energy cosmic rays. The detecting media to be used in a particular application have to be carefully selected as function of particle type and energy.

Instruments for radiation detection evolve as new technologies become available and, as a consequence, more and more sophisticated devices are

*An incoming particle is sometimes referred to as primary, while particles (or photons) produced or emitted in the interaction are sometimes referred to as secondary.

[†]The electromagnetic spectrum is subdivided into frequency regions, i.e., radiowaves, microwaves, infrared radiation, visible radiation, violet and ultraviolet radiation, X-rays and γ -rays.

made available to users, nowadays. For instance, complex, large and advanced instrumentation can be found in usage for applications ranging from nuclear medicine and health physics to experimental high energy particle and space physics.

In practice, books on instrumentation have to be oriented to application fields. Nevertheless, in order to understand the principle of operation of radiation detectors, a deep knowledge of the radiation interaction with matter is required. Physical phenomena allowing detection often involve soft electrons or photons, or atomic and molecular excitations. This is the case even for energetic and very energetic incoming charged particles. Furthermore, except for the case of total absorption of the incoming particle like in high-energy physics calorimetry, the particle is assumed to lose only a small fraction of its energy inside the detecting medium.

The loss of energy by a charged particle is caused by the interaction of the electric field associated with the moving charge and the one generated by the electronic (and, in few cases, nuclear) structure of detecting media. This process is referred to as *energy loss process* and allows to dissipate energy inside the detecting medium itself.

For sufficiently extended absorbers, high-energy hadronic particles (see Sect. 1.2) deposit their energy through a series of strong interactions with nuclei or nuclear constituents of the detector absorbing medium. The emerging particles will lose their energy by subsequent strong interactions but mostly by energy loss processes. Thus, a cascade of particles is generated and their energies are fully absorbed in the detecting medium. Similarly, electromagnetic cascades are generated by primary electrons, positrons and photons whose energy is degraded by electromagnetic interactions and energy loss processes.

The fundamental mechanism on which radiation detectors are based is the dissipation of a fraction (or, as above mentioned, the whole amount in some type of large detectors) of the incoming radiation energy inside the detecting material. The transferred energy is distributed among excited states, which are capable of generating *carriers* (for instance electrons-holes in semiconductors, ion pairs in gaseous devices, photons in scintillating media, etc.). These *carriers* are processed by appropriate readout elements (for instance front-end electronics for semiconductor detectors and for gaseous devices, or photomultipliers for scintillating materials, etc.). Hence, the required radiation information (such as momentum, energy, velocity) can be obtained.

For instance, in gas based detectors, the energy dissipation process re-

sults in creating *ion pairs* (i.e., electrons and positive ions) which are separated and move under the influence of an applied external electric field. Typically about 30 eV are required to create an ion pair. However, due to the limited number of ion pairs generated in a low density medium like a gas, a multiplication is usually needed in order to have enough carriers to induce a charge signal in the readout electronics. In semiconductor detectors, the medium is denser and an *electron-hole pair* requires about 3.6 eV to be generated. Usually, no multiplication is needed inside this device. In scintillating materials, whose densities are typically about half of semiconductor densities, the energy dissipation process results in emitting photons (about 100 eV are needed to emit a photon), a fraction of which can be conveyed onto a photomultiplier photocathode where, in turn, *photoelectrons* are emitted and subsequently multiplied.

1.2 Particles and Types of Interaction

Nowadays, it is usual to omit the term *elementary* while referring to the so-called *elementary particles* in fields like particle and nuclear physics. In the first half of the past century, only a few particles (among them the proton, neutron, electron, neutrino and photon) were known. At present, we know that these particles are final products from the interactions and decays of a very large number of particle states. This multitude of particles is proved to derive from a few fundamental constituent *fermions* of *spin* $\frac{1}{2}$, i.e., the *quarks* with fractional electric charges ($+\frac{2}{3}e$ and $-\frac{1}{3}e$, where e is the electron charge) and the *leptons* (like the electron and its corresponding neutrino) with integral electric charge or neutral. For instance, neutrons and protons are built from a set of three quarks. These constituents interact by exchanging *spin* 1 *bosons*, which mediate three types of fundamental interactions: strong, electromagnetic and weak interactions. A fourth interaction, gravitation, is mediated by a *spin* 2 *boson* (*graviton*). The *photon* mediates the electromagnetic interaction, W^\pm and Z the weak interaction, and the *gluon* the strong interaction.

Particles interacting via the *strong interaction* are known as *hadrons*. There are two main classes of hadrons: the *baryons*, with half-integral spin values, and the *mesons*, with integral spin values. For example, protons and neutrons are baryons, while pions are mesons. Protons and neutrons are constituents of nuclei and often referred to as *nucleons*. The strong interaction also provides the necessary binding forces to hold to-

gether nucleons inside the nucleus. Most of hadrons are unstable and are called *hadronic resonances*.

The *electromagnetic interaction* is usually responsible for most of non-nuclear interactions in physics beyond the *gravitational attraction*, and generates bound states in atoms and molecules. The Quantum Electrodynamics Theory (*QED*), one of the most successful theory in physics, allows extremely precise calculations of electromagnetic interactions of particles. *Weak interactions* are, for instance, responsible for processes like radioactive β -decays in nuclear physics. The gravitational force is the interaction involving massive bodies at very large distances. However, the gravitational force has negligible effect in particle–particle interaction at short distances.

The relative strengths of interactions at distances of $\simeq 10^{-18}$ cm are (see [Fernow (1986)] and references therein):

- strong interaction: 1
- electromagnetic interaction: $\approx 10^{-2}$
- weak interaction: $\approx 10^{-5}$
- gravitational interaction: $\approx 10^{-39}$

There is solid evidence that part of, if not all, the interactions are *unified*, i.e., are different aspects or manifestations of one single interaction. For instance, the electromagnetic and weak interactions have been unified in the *electroweak theory*, whose prediction of the existence of massive *gauge bosons*, W^\pm and Z , has been experimentally verified.

Another remarkable feature of nature is the existence of *antimatter*. For every particle (fermion or boson), there exists an antiparticle, which has the same mass and spin, but opposite values of electric charge and magnetic momentum. An example of antiparticle is the positron, which is the antiparticle of the electron.

It is customary (see for instance [Fernow (1986); Perkins (1986)] and Section 37 of [PDB (2002)]) to measure energies in *Mega* or *Giga* electron Volt (MeV or GeV) and to use conversion factors in such a way the constant speed of light c and \hbar are set to 1 to simplify relativistic calculations.

Then, the momenta are in units of MeV/c or in GeV/c and the masses in units of MeV/c² or GeV/c².

1.2.1 Quarks and Leptons

At present, experimental data support the picture in which the matter is built from two basic types of fermions, i.e., quarks and leptons. As mentioned before, quarks carry fractional electric charges ($+\frac{2}{3}e$ and $-\frac{1}{3}e$). Antiquarks carry opposite electric charges. There are different types of quarks distinguished by their *flavor*, i.e., u , d , s , c , b and t quarks. Their masses range from $\simeq 5 \text{ MeV}/c^2$ for the lightest quark (u) to $\approx 180 \text{ GeV}/c^2$ for the heaviest quark (t). Baryons are built from three quarks, while mesons from quark-antiquark pairs. Ordinary matter is usually constituted of baryonic particles, like protons (stable) and neutrons (unstable). Mesons are unstable.

Leptons carry integral electric charges. Three types of negatively charged leptons are known: the electron (e), the muon (μ) and the tau (τ), whose masses are 0.511, 105.7 and 1777 MeV/c^2 , respectively. Their antiparticles are positively charged. Associated with negative leptons are neutrinos, which are neutral leptons: ν_e (with mass $< 3 \text{ eV}$), ν_μ (with mass $< 0.19 \text{ MeV}$) and ν_τ (with mass $< 18.2 \text{ MeV}$). Neutrinos are longitudinally polarized with helicity $-\frac{1}{2}$ with regard to the direction of motion (they are *left handed*), while their correspondent antiparticles are *right handed* with helicity $+\frac{1}{2}$.

Charged leptons undergo both electromagnetic and weak interactions, while the neutrinos only undergo weak interactions. Quarks can interact via electromagnetic, weak and strong interactions.

1.3 Relativistic Kinematics

In this section, we will recall a few basic formulae of relativistic kinematics. In addition, we will discuss the relativistic kinematics of the two-body collision process and the invariant mass of systems of particles.

In relativistic mechanics, the *momentum* \vec{p} of a material point of mass m_r and velocity \vec{v} is $\vec{p} = m_r \vec{v} = m_r \vec{\beta} c$, where

$$\vec{\beta} = \frac{\vec{v}}{c}, \quad (1.1)$$

is the ratio between the material point velocity and the speed of light c . The mass m_r is also referred to as the *relativistic mass* and is related to the *rest mass*, m_0 , by the so-called *Lorentz factor* γ :

$$m_r = \gamma m_0, \quad (1.2)$$

where

$$\gamma = \frac{1}{\sqrt{1-\beta^2}} \quad \left(\text{conversely, } \beta = \frac{\sqrt{\gamma^2-1}}{\gamma} \right). \quad (1.3)$$

For the *total energy*, E , both the rest mass and the momentum have to be taken into account:

$$E = \sqrt{m_0^2 c^4 + p^2 c^2}, \quad (1.4)$$

or, equivalently from Eqs. (1.1–1.3)

$$\begin{aligned} E &= \sqrt{m_0^2 c^4 + m_r^2 \beta^2 c^4} \\ &= \sqrt{m_0^2 c^4 + (\gamma m_0)^2 \beta^2 c^4} \\ &= m_0 c^2 \sqrt{1 + \beta^2 \gamma^2} \\ &= \gamma m_0 c^2 \end{aligned} \quad (1.5)$$

$$= m_r c^2. \quad (1.6)$$

The *kinetic energy* is given by

$$E_k = E - m_0 c^2. \quad (1.7)$$

The energy and the momentum of a particle in a second reference system, whose constant velocity is $-\vec{\beta}_0 c$ with respect to the original system, are obtained by the so-called *Lorentz transformations* (see for instance [Hagedorn (1964)]):

$$\begin{aligned} \vec{p} &= \vec{p}' + \vec{\beta}_0 \gamma \left(\frac{\gamma}{\gamma+1} \vec{\beta}_0 \cdot \vec{p}' + \frac{E'}{c} \right) \\ \frac{E}{c} &= \gamma \left(\frac{E'}{c} + \vec{\beta}_0 \cdot \vec{p}' \right), \end{aligned}$$

where E' and \vec{p}' are the energy and the momentum in the original reference system. Furthermore, under Lorentz transformations, a time interval τ elapsed in a coordinate system, where the particle is at rest, is dilated by the Lorentz factor in a coordinate system moving with a velocity $-\beta c$ with respect to the particle (namely in the system in which the particle moves with a speed βc):

$$t = \gamma \tau. \quad (1.8)$$

For example, in its rest frame, a charged pion with rest mass ≈ 139.57 MeV/ c^2 has a mean-life of $\approx 2.6 \times 10^{-8}$ s. From Eq. (1.8), at 10 GeV in the laboratory frame (i.e., $\gamma \approx 72$ and $\beta \approx 1$), it becomes $t \approx 72 \times 2.6 \times 10^{-8} \approx 1.87 \times 10^{-6}$ s. Its path l , before decaying, is $l = ct \approx 562$ m.

1.3.1 The Two-Body Scattering

Radiation processes, like the ones resulting in energy losses by collision, take place in matter and can be considered (see following chapters) as two-body scatterings in which the target particle is almost at rest. In this section, we will study the kinematics of these processes and, in particular, derive equations regarding the maximum energy transfer.

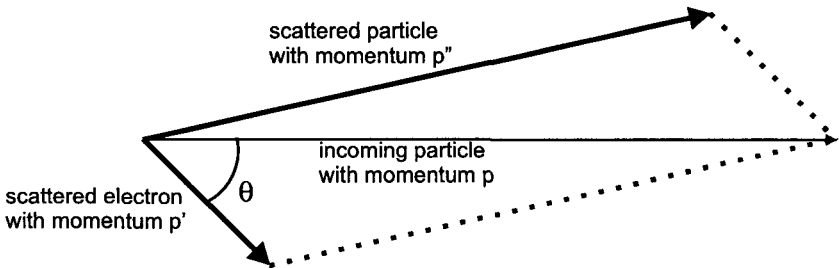


Fig. 1.1 Incident particle of mass m and momentum \vec{p} emerges with momentum $\vec{p}'' = |\vec{p}''|$, while the scattered electron emerges with momentum $\vec{p}' = |\vec{p}'|$.

Let us consider an incident particle (e.g. a proton, π , K, etc.) of mass m and momentum \vec{p} , and a target particle of mass m_e [Rossi (1964)] at rest. For collision energy-loss processes, the target particle in matter is usually an atomic electron (see Fig. 1.1). After the interaction, two scattered particles emerge: the former with mass m and momentum \vec{p}'' and the latter with mass m_e and momentum \vec{p}' . The latter one has the direction of motion (i.e., the direction of the three-vector \vec{p}') forming an angle θ with the incoming particle direction. θ is the angle at which the target particle is *scattered*. The kinetic energy [see Eq. (1.7)] of the scattered particle is related to its momentum by

$$E_k + m_e c^2 = \sqrt{p'^2 c^2 + m_e^2 c^4},$$

from which we get:

$$p'^2 = \frac{(E_k + m_e c^2)^2 - m_e^2 c^4}{c^2}. \quad (1.9)$$

The total energy before and after scattering is conserved, and we have

$$\sqrt{p^2 c^2 + m^2 c^4} + m_e c^2 = \sqrt{p'^2 c^2 + m^2 c^4} + E_k + m_e c^2,$$

and consequently

$$\sqrt{p'^2 c^2 + m^2 c^4} = \sqrt{p^2 c^2 + m^2 c^4} - E_k, \quad (1.10)$$

while from momentum conservation:

$$\vec{p}'' = \vec{p} - \vec{p}' \quad \Longrightarrow \quad p''^2 = p^2 + p'^2 - 2pp' \cos \theta. \quad (1.11)$$

Equation (1.11) can be rewritten taking into account Eq. (1.9):

$$p''^2 = p^2 + \frac{(E_k + m_e c^2)^2 - m_e^2 c^4}{c^2} - 2p \cos \theta \sqrt{\frac{(E_k + m_e c^2)^2 - m_e^2 c^4}{c^2}},$$

which becomes, after substituting p'' obtained from Eq. (1.10) and squaring both sides of that equation,

$$E_k \sqrt{p^2 c^2 + m^2 c^4} = -E_k m_e c^2 + pc \cos \theta \sqrt{(E_k + m_e c^2)^2 - m_e^2 c^4},$$

from which we get

$$pc \cos \theta \sqrt{\frac{E_k^2 + 2E_k m_e c^2}{E_k^2}} = m_e c^2 + \sqrt{p^2 c^2 + m^2 c^4},$$

and finally, by squaring both sides of the equation, we can derive the expression for the kinetic energy E_k of the scattered target particle, we have

$$E_k = \frac{2m_e c^4 p^2 \cos^2 \theta}{(m_e c^2 + \sqrt{p^2 c^2 + m^2 c^4})^2 - p^2 c^2 \cos^2 \theta}. \quad (1.12)$$

The kinetic energy E_k of the recoiling target particle is the amount of transferred energy in the interaction. From Eq. (1.12), we note that the maximum energy transfer W_m is for $\theta = 0$, i.e., when a head-on collision occurs. For $\theta = 0$, Eq. (1.12) becomes:

$$W_m = \frac{p^2 c^2}{\frac{1}{2} m_e c^2 + \frac{1}{2} (m^2 / m_e) c^2 + \sqrt{p^2 c^2 + m^2 c^4}}. \quad (1.13)$$

From Eq. (1.5), the incoming particle energy E_i is:

$$E_i = m\gamma c^2 = \sqrt{p^2 c^2 + m^2 c^4}.$$

We can rewrite Eq. (1.13) as:

$$W_m = 2m_e c^2 \beta^2 \gamma^2 \left[1 + \left(\frac{m_e}{m} \right)^2 + 2\gamma \frac{m_e}{m} \right]^{-1}. \quad (1.14)$$

For massive particles (e.g., proton,[†] K, π etc.), whose masses are much larger than the electron (or positron) mass, we have $m \gg m_e$ (≈ 0.511 MeV/c²). At sufficiently high energies, for which the incoming momentum p is $\gg \frac{m^2}{m_e} c$ (for instance for an incoming π with momentum $\gg 36$ GeV/c, or an incoming proton with momentum $\gg 1.7$ TeV/c), Eq. (1.13) becomes:

$$W_m \approx pc \approx E_i.$$

In the extreme relativistic case, a massive particle can transfer all its energy to the target electron in a head-on collision, i.e., a proton can be stopped by interacting with an electron.

At lower energies, i.e., when $p \ll \frac{m^2}{m_e} c$ (i.e., for an incoming π with momentum $\ll 36$ GeV/c, or an incoming proton with momentum $\ll 1.7$ TeV/c), the maximum energy transfer by a massive particle ($m \gg m_e$) [see Eq. (1.13)] is approximated by

$$W_m \approx 2m_e c^2 \left(\frac{p}{mc} \right)^2$$

and, because $p = m\beta\gamma c$, we have:

$$W_m \approx 2m_e c^2 \frac{\beta^2}{1 - \beta^2} = 2m_e c^2 \beta^2 \gamma^2. \quad (1.15)$$

For instance, a proton of 10 GeV has a Lorentz factor $\gamma \approx 10$ and $\beta \approx 1$. Thus, its maximum energy transfer is $W_m \approx 100$ MeV.

1.3.2 The Invariant Mass

The four-momentum of a particle of rest mass m_0 is defined as $\vec{q} = (\frac{E}{c}, \vec{p})$. The scalar product between two four-momenta \vec{q} and \vec{q}' is an invariant (i.e., frame independent) quantity, and is given by (e.g. Section 37

[†]The rest mass of the proton is ≈ 938.27 MeV/c².

of [PDB (2002)]):

$$\bar{q} \cdot \bar{q}' = \frac{E E'}{c^2} - \bar{p} \cdot \bar{p}'. \quad (1.16)$$

The *invariant mass* of a particle is related to the scalar product of its four-momentum:

$$\bar{q} \cdot \bar{q} = q^2 = \frac{E^2}{c^2} - \bar{p} \cdot \bar{p} = \frac{E^2}{c^2} - p^2 = m_0^2 c^2,$$

and finally

$$m_0 = \sqrt{\frac{\bar{q} \cdot \bar{q}}{c^2}}. \quad (1.17)$$

For a single particle, its invariant mass is the same as the rest mass.

The invariant mass, M , of a set of particles is the energy available in their center of mass system. It is given by:

$$M = \sqrt{\frac{\bar{q}_s^2}{c^2}} = \sqrt{\frac{[\sum_i (E_i/c)]^2 - (\sum_i \vec{p}_i) \cdot (\sum_i \vec{p}_i)}{c^2}}, \quad (1.18)$$

where the total four-momentum, \bar{q}_s , is given by

$$\bar{q}_s = \sum_i \bar{q}_i.$$

For instance, let us consider two particles with masses m_1 and m_2 and momenta \vec{p}_1 and \vec{p}_2 . From Eq. (1.18), we have that their invariant mass $M_{1,2}$ is:

$$\begin{aligned} M_{1,2} &= \frac{1}{c} \sqrt{\left(\frac{E_1 + E_2}{c}\right)^2 - p_1^2 - p_2^2 - 2p_1 p_2 \cos \theta} \\ &= \frac{1}{c} \sqrt{2 \frac{E_1 E_2}{c^2} + m_1^2 c^2 + m_2^2 c^2 - 2p_1 p_2 \cos \theta}, \end{aligned} \quad (1.19)$$

where θ is the angle between the three-vectors \vec{p}_1 and \vec{p}_2 . For example, let us take a proton of 100 GeV incident on a target proton at rest, like in a high-energy physics fixed target experiment. From Eq. (1.19), because $p_2 = 0$, $E_2 = m_2 c^2$, $m_1 = m_2 \approx 1 \text{ GeV}/c^2$, the available center of mass energy (i.e., the invariant mass) becomes

$$M_{1,2} \approx \sqrt{200 + 1 + 1} \approx 14.2 \text{ GeV}/c^2.$$

In the scattering between an incoming particle 1 and a target particle 2, we indicate (with the variable s) the invariant quantity:

$$s = (\bar{q}_1 + \bar{q}_2)^2 = m_1^2 c^2 + m_2^2 c^2 + 2 \frac{E_1 E_2}{c^2} - 2 \vec{p}_1 \cdot \vec{p}_2. \quad (1.20)$$

If the particle 1 (2) emerges as particle 3 (4), the invariant quantity s is also given as:

$$s = (\bar{q}_3 + \bar{q}_4)^2.$$

From Eq. (1.19), s is the invariant mass square of the system 1,2 (3,4) times c^2 , i.e., the square of the total energy in the center of mass system divided by c^2 . For the same reaction, we define the invariant quantity t as the square of four-momentum transfer:

$$t = (\bar{q}_1 - \bar{q}_3)^2 = (\bar{q}_2 - \bar{q}_4)^2 = m_1^2 c^2 + m_3^2 c^2 - 2 \frac{E_1 E_3}{c^2} + 2 \vec{p}_1 \cdot \vec{p}_3. \quad (1.21)$$

Both s and t are called *Mandelstam variables*.

1.4 Cross Section and Differential Cross Section

The cross section, σ , for a physical process is derived from the reaction probability for the occurrence of such an interaction. More precisely, when a collimated particle beam impinges on a target (see Fig. 1.2), some particles are removed by the physical reactions, resulting in an attenuated beam. The physical reactions occurring between the beam and the target particles include for example elastic scattering and particle production. A net difference between the incoming and outgoing particles can be measured and the removal probability of beam particles can be determined.

The simplest way of representing such a reaction is to imagine the incoming beam made of a uniform distribution of particles and the target as made of a disk onto which a certain amount of beam particles interact. This way, particles impinging onto the disk surface interact, while particle outside this surface continue their trajectory unaffected. However, this naive point of view has to account for the finite dimensions of both projectiles and target. This disk does not coincide with the *geometrical section* presented by the target and depicted by $\sigma_g = \pi R_g^2$ in Fig. 1.2, where R_g is the physical (i.e., geometrical) radius of the target. It means the *effective area* experienced by incoming point-like particles. This effective area is the so-called *total reaction cross section* (σ_{total} in Fig. 1.2) and takes into account

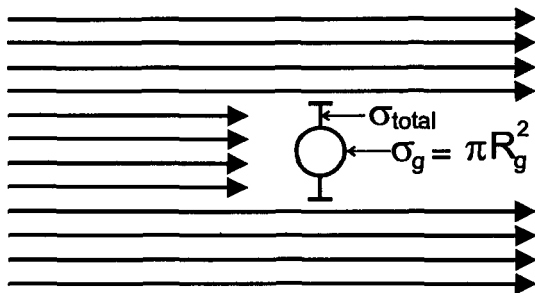


Fig. 1.2 Reaction and geometrical cross sections (see for instance [Marmier and Sheldon (1969)]).

the different types of reactions (often referred to as *partial cross sections*) between the projectile and the target. In interactions among particles, or particles and nuclei, or particles and atoms, the cross section size is usually expressed in units of *barn* indicated by *b* (see Appendix A.1):

$$1 \text{ b} = 10^{-24} \text{ cm}^2 = 10^{-28} \text{ m}^2.$$

Let us have a monochromatic beam of F_0 particles, for which σ_{total} is the total atomic cross section for all interaction processes between incoming particles and target atoms inside the absorber. In addition, we suppose that the overall absorber thickness is such that the probability of double particle interaction can be neglected. In the passage through a thickness dx' of the medium, the number of removed particles $-dF$ (the minus sign indicates that particles are removed from the beam) is proportional to the number of the beam particles F' at the depth x' and to the number of target atoms per unit of volume, n_A , of the traversed material:

$$-dF = F' P_{int},$$

where $P_{int} = (\sigma_{total} dx') n_A$ is the probability of removing a particle in the thickness dx' . It has to be noted that n_A is the reciprocal of the atomic volume. We have:

$$-dF = F' (\sigma_{total} dx') n_A = F' (\sigma_{total} n_A) dx' = \frac{F'}{\lambda_{col}} dx',$$

where

$$\lambda_{col} = \frac{1}{n_A \sigma_{total}}. \quad (1.22)$$

The coefficient λ_{col} has the dimension of a length and is the so-called *collision length*, i.e., it is the *mean free path* between successive collisions. As a consequence, by traversing a thickness x of the absorber, we have:

$$\frac{dF}{F'} = -\frac{1}{\lambda_{\text{col}}} dx' \Rightarrow \int_{F_0}^F \frac{dF}{F'} = \int_0^x -\frac{dx'}{\lambda_{\text{col}}} \Rightarrow \ln \frac{F}{F_0} = -\frac{x}{\lambda_{\text{col}}},$$

and finally

$$F = F_0 \exp \left[-\left(\frac{x}{\lambda_{\text{col}}} \right) \right]. \quad (1.23)$$

Thus, there is an exponential decrease of the number of particles upon the passage in the absorbing medium

The value of n_A , in units of cm^{-3} , is given by

$$n_A = \frac{N\rho}{A}, \quad (1.24)$$

where N is the *Avogadro constant* (see Appendix A.2), ρ is the absorber density, in g/cm^3 , and A is the *atomic weight*. Whereas, the *number of electrons per cm^3* , n , is given by

$$n = Zn_A = \frac{ZN\rho}{A}, \quad (1.25)$$

where Z is the *atomic number*, i.e., the number of protons inside the nucleus of that atom.

From Eqs. (1.22, 1.24), the collision length can be rewritten as:

$$\lambda_{\text{col}} = \frac{A}{N\rho\sigma_{\text{total}}}. \quad (1.26)$$

An interaction, which results in the emission of a reaction product, can depend on parameters like the incoming energy or the emission angle. Therefore, we can introduce the so-called *differential cross section* to express the emission probability dependence on these parameters. For instance, the differential cross section per unit of solid angle $\frac{d\sigma}{d\Omega}$ gives, once multiplied by the solid angle element $d\Omega$, the incoming particle cross section to yield the reaction product into the element of solid angle $d\Omega$ lying at a mean angle θ with respect to the incident beam direction (the so-called *scattering angle*) and at a mean *azimuthal angle* ϕ . We have:

$$\sigma = \int_0^\Omega \frac{d\sigma}{d\Omega} d\Omega = \int_{\phi=0}^{2\pi} \int_{\theta=0}^{\pi} \frac{d\sigma}{d\Omega} \sin \theta d\theta d\phi,$$

where σ is the cross section for the reaction and $d\Omega = \sin \theta d\theta d\phi$.

1.4.1 Atomic Weight and Atomic Mass Unit

The atomic weight A of an element is determined by its isotopic abundance [Tuli (2000); NNDC (2002a)] in the Earth's surface and is relative to the mass of the ^{12}C isotope, defined to be exactly 12 unified atomic mass units (indicated by the symbol u, see Appendix A.2) as adopted by the International Union of Pure and Applied Chemistry (IUPAC) in 1966. In this scale, hydrogen has an atomic weight of 1.00794 u (see Appendix A.3 and references therein).

1.5 Detectors and Large Experimental Apparata

Radiation detectors use *detecting* (sometime referred to as *active*) *media* and *readout* systems. The operation of any detecting device is based on specific effects of radiation interaction in matter. These effects are exploited in order to produce quantitative measurable signals in the readout system associated with the detection system itself.

The basic features of radiation detectors can be understood once fundamental processes of radiation interaction in matter are considered (see chapters on *Electromagnetic Interaction of Radiation in Matter* and on *Nuclear Interactions in Matter*). For instance, the collision energy loss is the mechanism generating primary electrons (which in turn can generate secondary electrons) in gaseous detectors, or excited molecules (which decay emitting photons) in scintillating devices, or generated electron-hole pairs in semiconductors, etc. The primary mechanism of transferring energy from an incoming charged particle to a medium has to be capable of generating secondary detectable particles, whose number or flux of energy has to be as much as possible linearly related to the incoming number of particles or incoming particle energy. Radiation detectors, or combinations of them, can provide a wide range of information as spatial locations, particle momentum, velocity, energy, etc.

For instance, in nuclear medicine, the image formation is based on the spatial reconstruction of the radiation emitted from a patient. The detecting system needs to be complex and consists of many subdetectors in order to cover large emission area and provide a 3-dimensional reconstruction of the internal volume of the patient under investigation.

In high-energy physics experiments, detectors are located downstream a fixed target or surrounding the collision point in colliding beams machines. In space experiments, sets of highly reliable detectors are located on board of satellites and recently on board of the International Space Station for photons and energetic cosmic rays detection. Particles created in high energy collisions or impinging on a space detector, pass through various kinds of detectors whose tasks are different. Examples are:

- tracking, with capability of momentum analysis in *magnetic spectrometers*
- electron and hadron separation
- particle identification
- energy determination
- triggering
- data acquisition
- monitoring

Each subdetector has very specific characteristics and its functionality has to be optimized taking into account the features of other subdetectors.

Particles passing through tracking detectors (or *trackers*) have their trajectories reconstructed by dedicated computer software codes. The accuracy of reconstructed trajectories depends on the spatial resolution of the tracker, which can be of a few μm 's for semiconductor detectors (see the chapter on *Solid State Detectors*), $\approx 100 \mu\text{m}$ for drift chambers and a few hundreds μm 's for MultiWire Proportional Chambers (*MWPC*). The two latter ones are gas based devices. The accuracy also depends on the multiple Coulomb scattering inside the tracker. In *magnetic spectrometers*, the particle momentum can be determined once the particle trajectory has been reconstructed.

As will be discussed in details in this book, electrons, photons and hadrons can create electromagnetic and hadronic showers in matter (see Sects. 2.4 and 3.3). The characteristics of the shower can be determined with calorimeters, as discussed in the chapter on *Principles of Particle Energy Determination*. These detectors can measure both the energy and the impact position of the incoming particle. In addition, the energy deposition distribution along and perpendicularly to the incoming particle direction is used to discriminate among incoming electrons/photons and hadrons.

Other devices, such as the *Transition Radiation Detectors (TRD)*, can provide signatures for discriminating electrons from hadrons at high energy. These devices are classified among the so-called *particle identification*

detectors, like the *Čerenkov detectors*.

All the detectors or subdetectors in an experiment or in a large, complex detection system must be carefully integrated. The design system does not need to exploit all the best subdetector features. It only needs to make them suited to the purpose of the overall resulting apparatus. Fast outputs from subdetectors or dedicated detectors provide *trigger signals*, which indicate that a particular type of *event* has occurred inside the apparatus. The trigger looks for spatial and/or temporal correlation of detectors or subdetector signals, which have been set in designing the apparatus. The trigger can also be based on threshold, such as energy threshold.

Calibration and on-line monitoring are tasks which have to be particularly investigated and implemented in large and complex apparatus. Data are usually collected via a *data acquisition system (DAQ)*, which sends them or a part of them to monitoring computer codes and to the recording system.

Computers play a central role in processing data and afterwards in displaying processed data. Much of the software code used in the reconstruction of physical events is detector or apparatus dependent. Graphical routines for data display are by themselves an important field of continuous development and require more and more powerful processors.

1.5.1 *Trigger, Monitoring, Data Acquisition, Slow Control*

A trigger signal is an electronic signal which indicates the occurrence of an *event* which has to be processed and, possibly, collected by the data acquisition part of the apparatus. A well designed trigger avoids the data collection system to be swamped by similar but background events. This way, expected events together with a minimal amount of background events will be collected and processed. For instance, the trigger can be constructed to identify particles, to separate electrons from hadrons, to count the event multiplicity, etc. For large apparatus, the trigger is organized with a few levels following a hierarchical sequence. Programmable devices are commonly employed such as look-up tables, hard-wired processors, microprocessors, emulators.

In recent years, the pipelined processing has been often adopted in order to avoid loss of information. It is typically employed for event recording and storage in high performance computing systems. There are different types of pipelines for storing signals coming from various parts of the apparatus. The pipeline can be both analog and digital.

Particularly interesting events, as well as events sampled on a statistical basis, can be passed to the on-line event display task. This latter task can be integrated inside the on-line monitoring and calibration tasks, which allow us to verify that the whole detector is properly functioning during the data collection. Within this framework, automatic processes search for anomalous behaviors of subdetectors and send warning messages or try to readjust remote controlled subdetector elements to restore the working condition. Sets of calibration constants are also collected in systematically updated databases and used in reconstruction procedures.

The term “data acquisition” includes the data collection from the whole apparatus, data storage on accessible media and subsequently to external software codes for reconstruction and display.

Complex detector systems usually require that subdetector operations and re-adjustments be carried out by dedicated remote software codes. Independently, if the event has to be considered or not as a background event, subdetector operations are expected to be performed properly when some detector parameters are within predefined value ranges. These quantities are for instance high voltages and currents of subdetectors, flow of gases (for gaseous detectors), temperature distribution, etc. The slow control includes the recording, monitoring and control of all parameters which are expected to be within predefined ranges during the data collection.

1.5.2 *General Features of Particle Detectors and Detection Media*

The spatial resolution depends on the detector type and, among detectors using similar media, on the type of readout system. Both the *resolution time* and the *dead time*[§] also depend on the detector type. Fast *drift chambers* have resolution times of $\simeq 2$ ns and dead times of $\simeq 100$ ns. Scintillator devices can reach resolution and dead times of about (100–150) ps and 10 ns, respectively. *Photographic emulsions* have spatial resolution of $\simeq 1$ μm . *Silicon strip* and *silicon pixel detectors* can achieve spatial resolutions of \simeq a few mm and 2 μm respectively.

The *photomultiplier* is a suitable vacuum tube designed both as a source of primary electrons (*photoelectrons*) emitted by the photocathode and as an electron amplification by secondary emission process. The amplification factor can be as large as 10^6 . Photomultipliers are widely used in associa-

[§]The dead time is the time during which a detector is not capable of detecting a next coming particle.

tion with detection media in which photons are emitted, like scintillators and Čerenkov detectors. Photomultiplier operations can be limited, or even completely impaired, inside strong magnetic fields.

Organic scintillators are classified as organic crystals (i.e., anthracene, naphthalene, etc.), liquids[¶] or plastics^{||} depending on the type of the scintillating medium in usage and their densities are between $\simeq (1.03\text{--}1.25)$ g/cm³. The scintillation mechanism is particularly noticeable in organic substances containing aromatic rings, for instance polystyrene, polyvinyltoluene and naphthalene. In liquid scintillator, molecules of toluene and xylene are typically included. About 3% of the deposited energy is re-emitted as optical photons. By far, the plastic scintillators are the most widely employed. Photon emission yields are approximately 100 eV of energy deposited inside the scintillating medium (see chapter on *Scintillating Media and Scintillator Detectors*). A *minimum ionizing particle* (see the definition on page 38) can generate up to 2×10^4 photons traversing ~ 1 cm of plastic scintillator. However, only a small fraction, typically less than 10%, of the generated photons arrive on the photomultiplier photocathode, whose *quantum efficiency* (i.e., the probability of emitting a photoelectron per impinging photon) does not exceed $\sim 30\%$ for the most favorable photon frequency. In addition, local ionizations much larger than those generated by minimum ionizing particles emit less light. Plastic scintillators are reliable and robust. However, their light yield degrades due to aging effects. For instance, aging can be enhanced by exposure to solvent vapors, irradiation and mechanical flexing. The radiation damage depends not only on the integrated dose, but on the dose rate, and environmental factors (like temperature and atmosphere) before and after the irradiation, as well as on material properties. Commonly used inorganic scintillators have larger densities, between $\simeq (3.67\text{--}8.28)$ g/cm³. They are employed when large densities and good energy resolution are required.

Detectors using a gas, or more likely a mixture of gases, have undergone a great deal of development since the first planar detector geometry: the MWPC (MultiWire Proportional Chamber), realized a few decades ago. This planar geometry has allowed to exploit the cylindrical gas detector properties (see the chapter on *Ionization Chambers*) regarding both the small electron multiplication volume around the anode wire and the large drift volume available to positive ions at almost constant electric field

[¶]In a liquid scintillator an organic crystal (solute) is dissolved in a solvent.

^{||}Plastic scintillators are similar in composition to liquids. Polystyrene and polyvinyltoluene are commonly used as base plastics to replace the solvent.

towards the cathode. In the detector, ion pairs are generated in a gas layer, whose thickness is typically between a few cm's and a fraction of a cm. Anodes are regularly separated by less than 2 mm, but not much less than 1 mm, because there are practical difficulties of precisely stringing wires below 1 mm and in addition the mechanical tension, balancing the electrostatic force between wires, cannot exceed its critical value. This allows the achievement of spatial resolutions up to a few hundreds μm . These detectors need an individual readout channel per anode. Similar or even better spatial resolutions, with a small readout channel density, can be achieved with the so-called *drift chambers*. In these devices, the position of the passing particle is determined by the time difference between the passage of the particle and the arrival of electrons at the wire. Detectors (the so-called *time projection chamber*) with long drift distances perpendicularly to a multi-anode proportional plane provide three-dimensional information. Large volume chambers up to a few tens of m^3 and several thousands of wires have been successfully operated in high energy physics experiments. The anode spacing limitation can be overcome by using lithographic technique, which have been able to produce a miniaturized version of a MWPC with thin aluminum strips engraved in an insulating support and an anode spacing reduced to (0.1–0.2) mm.

Silicon detectors are the most widely used semiconductor detectors. They are *p-n junction* diodes operated at reverse bias (see chapter on *Solid State Detectors*). Their substrate is typically *n*-type high resistivity silicon with thickness between (300–500) μm . Full depletion voltages are usually between (50–150) V for 300 μm thick detectors. The energy needed to be deposited inside the detector active volume to create an *electron-hole* (*e-h*) pair is about 3.6 eV. Electrons and holes are referred to as *carriers*. A minimum ionizing massive particle** loses on average approximately 30 keV per 100 μm in a silicon detector,^{††} i.e., it generates approximately 83 *e-h* pairs/ μm . The *transit time*, i.e., the time needed by carriers to drift towards the electrodes and, consequently, to induce electric signals on them, decreases as the reverse bias voltage necessary for full depletion increases. Typical transit times are ≤ 10 ns for electrons and ≤ 25 ns for holes in the case of a fully depleted 300 μm thick device. The transit time is mainly limited by the carrier mobility saturation for electric field larger than $\approx 10^4$ V/cm. In the beginning of the 1960s, the first demonstrations

**A massive particle is at the energy-loss minimum for $\beta\gamma \approx 3$ (see page 38).

††Since fast δ -rays are not fully absorbed in thin absorbers, the average energy loss per 100 μm can depend on the detector thickness, see Sect. 2.1.1.3.

were made that silicon detectors operated at room temperature could be used for nuclear reaction studies and spectroscopy. Since then, a great deal of work and combined efforts have been carried out, making this type of detectors more and more reliable and easy to operate. Up to the beginning of the 1980s, these devices were expensive and with active areas not exceeding a fraction of 1 cm². At that time (see for instance [Rancoita and Seidman (1982)]), the need to use them in high-energy physics experiments has resulted in developing large area *strip silicon detectors*, at relatively low cost. A further important step was the development of monolithic front-end electronics. Thus, a high density of readout channels (for instance one readout channel every 50 μm) could be achieved. Their usage as tracking devices has allowed the construction of complex detectors with some m² of overall active area. A subsequent development has achieved a three-dimensional readout by employing both the so-called *pixel silicon detectors* and the *double sided silicon detectors*.

As discussed in the chapter on *Principles of Particle Energy Determination* (see for instance [Leroy and Rancoita (2000)] and references therein) around mid-eighties, high energy sampling calorimeters using silicon detectors as active medium were developed for particle physics experiments. This way, very large active areas of silicon detectors have been realized for both high energy and space physics applications.

Silicon diodes can be used as photodiodes. Their quantum efficiencies are > 70% for photon wavelengths between ~ 600 nm and 1 μm . In practical applications, for instance in detecting photons from a scintillator, attention has to be paid to make sure that the detected signal due to photon conversion is larger than that due to the energy loss of particles traversing simultaneously the photodiode.

Both silicon detectors and photodiodes can work properly even in strong magnetic fields.

Radiation damage can impair the silicon device performance. Nevertheless, if properly designed and associated with suited front-end electronics, it can keep its performance in large radiation fluence environments. Radiation damage causes the creation of *Frenkel pairs*, i.e., pairs consisting of a displaced atom from a lattice site and the corresponding vacancy in the previously occupied lattice site. This leads to a dose dependent increased leakage current, to the creation of deep and shallow defects which can act as carrier trapping centers, to the build up of space charge able to change (i.e., to highly increase) the required reverse bias for full depletion, etc. In addition, there are surface damages resulting in an increase of the sur-

face leakage current. In strip detectors, the inter-strip isolation is usually affected.

Particle identification detectors are designed to determine the particle rest mass m_0 once the measurement of particle momentum $p = m_0\beta\gamma c$ (see page 6) has been performed by other detectors. At low energy, e.g. for nuclear and particle physics applications, the particle velocity ($= \beta c$) can be measured by using the *time-of-flight* technique, i.e., by determining how much time it takes for the particle to pass through two subsequent detectors. For instance, time-of-flight systems using two plastic scintillators 1 m apart are able to provide a good particle mass identification for electrons, pions, kaons and protons up to particle momenta of $\approx (1.5\text{--}2)$ GeV/c for time resolutions of $\approx (120\text{--}150)$ ps.

Čerenkov detectors exploit the properties of the Čerenkov radiation (described in Sect. 2.2.2), which depends on the particle velocity. Threshold Čerenkov counters provide an information whether the particle is above or below the threshold velocity for emitting Čerenkov radiation in the radiator medium. Differential Čerenkov counters exploit the dependence on both the particle velocity and the emission angle of the emitted radiation. Finally *Ring Imaging Čerenkov Detectors (RICH)* exploit the properties of the Čerenkov radiation in geometries up to the full solid angle. These devices typically include more than one radiator medium.

Transition radiation (described in Sect. 2.2.3) is emitted when a charged particle crosses the boundaries of two media with different dielectric constants. Emitted photon energies depend both on the medium plasma frequency and on the *Lorentz factor* γ of the particle. In practice, the transition radiation becomes useful for particle detection when Lorentz factors are larger than 1000. The transition radiation devices are usually employed to provide electron/hadron separation in the energy range $0.5 \leq p \leq 100$ GeV/c, when soft *X*-rays radiated by electrons have energies of some keV's and can be detected inside wire chambers operated with gas mixtures containing xenon. A *Transition Radiation Detector (TRD)* is typically composed of several modules, each made of an *X*-ray detector and a radiator. The radiator is subdivided in order to have several hundred boundaries, because the photon probability emission is of $\simeq 1\%$ per boundary crossing. The TRD performance depends on its overall length.

The development of electromagnetic and hadronic showers is described in Sects. 2.4 and 3.3, respectively. These showers differ largely both for their longitudinal (i.e., along the incoming particle direction) and transversal (i.e., on the plane perpendicular to the incoming particle direction)

shapes. By exploiting these characteristics, the electron/hadron identification is achieved in calorimetry. *Calorimeters*, as discussed in the chapter on *Principles of Particle Energy Determination*, are devices in which the total incoming particle energy is deposited by a multiplicative process called *cascading shower development*. In homogeneous calorimeters, the incoming particle releases its energy in a medium which is at the same time the *passive absorber* shower generator and the *active detection medium*. These calorimeters can achieve the best energy resolution and are typically employed for particles depositing their energy by electromagnetic cascades. Sampling calorimeters, mostly used for high energy electromagnetic and hadronic showers, consist in passive absorbers interspaced with active detection media. This way, only a small fraction of the incoming particle energy, usually less than a few percents or even a fraction of percent, is deposited in the active part of the detection system. The *sampling fluctuations* are dominating the electromagnetic calorimeter energy resolution and are largely contributing to the overall hadronic calorimeter resolution. Because physical mechanisms by which energy is deposited in matter by electromagnetic and hadronic showers are different, in hadronic calorimetry care has to be given in equalizing the hadronic and the electromagnetic responses of the calorimeter, i.e., by achieving the so-called *compensation condition* (e.g. to achieve the ratio $e/\pi = 1$). In fact, contrary to electromagnetic cascades initiated by electrons and photons, cascades initiated by hadrons will proceed by generating both hadronic particles and particles showering via electromagnetic cascades, i.e., a hadronic shower will always contain some electromagnetic sub-cascades, due to the production in cascading of neutral particles (like π^0 , η , ...) decaying into photons. Electromagnetic sampling calorimeters typically have a response which is proportional to the incoming particle energy, E , and the energy resolution varies as $1/\sqrt{E}$. These features are present in compensating hadronic calorimeters. In this latter case, the energy resolution is worsened by the so-called *intrinsic fluctuations*, which take into account that a non negligible fraction of the incoming hadron energy is spent in breaking nuclear bounds, as for instance in nuclear spallation processes or in emitting largely undetected neutrons. In the calorimeter resolution, the extension of sampling fluctuations depends on both the type of passive absorbers and active media, as well as on the kind of calorimetric structure realized, for instance thicknesses of passive absorbers. Active media commonly employed are scintillators, liquid argon, silicon detectors, gas detectors, etc. Very large volume calorimeters (a few tens of m^3) have been constructed for high energy physics experi-

ments. Specialized and compact electromagnetic calorimeters with imaging capabilities have been flown in balloon experiments. For all these systems, calibration procedures have been designed and set into operation in order to keep constantly calibrated and controlled many thousands of readout channels.

The very low interaction cross section between Weakly Interacting Massive Particles, *WIMP*, and the nuclei of the detector's active medium requires the use of very massive detectors to achieve a sensitivity level allowing the detection of *WIMP*s particles in the galactic environment. The effective cost of these detectors has to be minimized. Superheated droplet detectors, referred to as "bubble detectors" (see chapter on *Superheated Droplet (Bubble) Detectors*), of low cost, offer an attractive solution to the problem of *WIMP* detection. These detectors use superheated freon liquid droplets (active material) dispersed and trapped in a polymerized gel. This detection technique is based on the phase transition of superheated droplets at room or moderate temperatures. The phase transitions are induced by nuclear recoils when undergoing interactions with particles. These detectors are threshold detectors, a minimal energy deposition has to be achieved for inducing a phase transition. Their sensitivity to various types of radiation strongly depends on the operating temperature and pressure. Over the years, bubble detectors have been developed using detector formulations that are appropriate for a range of applications such as the direct measurement of neutralinos predicted by minimal supersymmetric models of cold dark matter, or portable neutron dosimeters for personal dosimetry or the measurement of the radiation fields in irradiation zones near particle accelerators or reactors.

Most of the instrumentations and experimental techniques developed for particle, nuclear and space physics have been used in medical applications. Furthermore, in this book, particular attention is paid to the physics mechanisms of radiation interaction with matter. These mechanisms, treated in the chapters on *Electromagnetic Interaction of Radiation in Matter* and on *Nuclear Interactions in Matter*, are of very important for the understanding of detectors and detector systems commonly used in nuclear medicine and in general for the *medical applications*. In the chapter on *Medical Physics Applications*, imaging techniques based on *Magnetic Resonance Imaging (MRI)*, *Single Photon Emission Computed Tomography (SPECT)* and the *Positron Electron Tomography (PET)* are treated. The main advantage of *MRI* is that no radioactive material is needed, i.e., it exploits the non-zero spin property of some nuclei. *MRI* uses magnetic fields

varying from 0.2 to 2 T and radio frequency waves to observe the magnetization change of the non-zero spin nuclei. The isotope of hydrogen, ^1H , which has a nuclear spin of $\frac{1}{2}$, is a major component of the human body and is used as the main source of information. Both *SPECT* and *PET* make use of properties of photon interactions in matter. For *SPECT*, the gamma-ray imaging technique proceeds through the injection to the patient of a radioactive substance which emits photons of well-defined energy. The distribution of radionuclides, position and concentration, inside patient's body is monitored externally through the emitted radiation deposited in a photon detector array rotating around the body and which allows the acquisition of data from multiple angles. *PET* is a nuclear medical imaging technique which relies on the measurement of the distribution of a radioactive tracer or radiopharmaceutical labeled with a positron emitting isotope injected into a patient. The positron emitted by the radioactive tracer or radiopharmaceutical annihilates very close to the emission point (≤ 1 mm) with an electron of the body to produce a pair of 511 keV photons emitted back-to-back, which in turn are detected by the *PET* camera.

It is important to note that many detectors rely partially or crucially on low-noise electronics. Most of the more visible and useful detector applications have been achieved through the usage of cheap monolithic electronics, designed and developed for fundamental physics researches and afterwards adjusted to other applications.